ISSN 2070-2051, Protection of Metals and Physical Chemistry of Surfaces, 2019, Vol. 55, No. 6, pp. 1226–1235. © Pleiades Publishing, Ltd., 2019.

PHYSICOCHEMICAL PROBLEMS OF MATERIALS PROTECTION

Corrosion Performance of AISI 304 Stainless Steel in CO_2-Saturated Brine Solution

H. Ruiz-Luna[a, *], J. Porcayo-Calderón[b], A.G. Mora-García[c], I. López-Báez[d], L. Martinez-Gomez[e], and J. Muñoz-Saldaña[c]

[a] *Conacyt–Universidad Autónoma de Zacatecas, Zacatecas, 98000 Mexico*
[b] *Universidad Autónoma del Estado de Morelos, CIICAp, Cuernavaca, Morelos, 62209 Mexico*
[c] *Centro de Investigación y de Estudios Avanzados del I.P.N., Libramiento Norponiente 2000, Real de Juriquilla, Querétaro, 76230 Mexico*
[d] *Universidad de Guanajuato, Ex–Hacienda San Matías s/n, Guanajuato, 36020 Mexico*
[e] *Instituto de Ciencias Físicas-UNAM, Av. Universidad s/n Col. Chamilpa, Cuernavaca, Morelos, 62210 Mexico*
**e-mail: hruizlu@conacyt.mx*

Received January 30, 2019; revised June 5, 2019; accepted June 13, 2019

Abstract—Corrosion behavior of 304 stainless steel exposed to a NaCl (3.5 wt %) solution saturated with CO_2 has been analyzed using electrochemical techniques including, potentiodynamic polarization, polarization resistance, and electrochemical impedance measurements. The stainless steel samples were evaluated having different surface and pre-oxidation treatments. The oxide scales formed on 304 stainless steel oxidized in different pO_2 at 1100°C have also been studied and compared. Different morphologies and chemical composition of the oxide scales were observed after oxidation at low and high oxygen partial pressures. Oxide layers with high chromium content were formed on the ground sample pre-oxidized in Ar while iron-rich oxides were mainly formed under air atmosphere. The electrochemical corrosion results indicate that non-oxidized 304 SS exhibits the best corrosion performance followed by the ground sample heat-treated in argon. For the oxidized stainless steels, the differences in the electrochemical responses are associated to the morphological characteristics and composition of the oxide layer. Homogeneous and dense Cr-rich oxide scale provides protection to 304 SS during exposure to CO_2-saturated solutions while the formation of Fe-oxides with porous morphology increases the corrosion rate of 304 stainless steel.

Keywords: electrochemical corrosion, stainless steel, oxide layer, Cr content, surface morphology
DOI: 10.1134/S2070205119060261

1. INTRODUCTION

Austenitic stainless steel is used for a variety of industrial applications due to its strength and excellent resistance to corrosive environments. For instance, this material is employed in combustion processes, components and devices of boilers, pipelines used in petroleum plants, water-cooled nuclear reactors, heat exchangers, oil, gas and geothermal power plants, and gasification systems [1–3]. The corrosion resistance of stainless steel (SS) depends mainly on the Cr content within the alloy because this element is responsible for the formation of a stable and protective chromium-rich oxide on the alloy surface [4–7]. For instance, T. Terachi et al. [5] reported a reduction in the corrosion rate of austenitic stainless steels in simulated pressurized water reactors as the Cr content increases as a consequence of the formation of a fine-particle chromium-rich scale adjacent to the metal surface.

In general, it has been accepted that the formation of a passive layer protects the metal surface from corrosive atmospheres reducing considerably its deterioration. However, under normal operation conditions, stainless steel is still susceptible to suffer uniform and/or local corrosion after long operation times, especially in CO_2 solutions [8, 9], because the corrosion rate of metals and alloys is strongly related to their ability to form a protective and adherent oxide layer [4, 10, 11].

Although stainless steels are Cr_2O_3-forming alloys, a protective and solely chromium scale that reduce the high and low temperature degradation of the metal is not always formed and maintained. During oxidation and/or corrosion exposures, several oxides, including Cr- and Fe-rich oxides, spinels, and oxides with large concentration of minor alloy constituents such as Mn, may grow predominantly on the SS surface depending on several variables such as initial material composition and treatments, Cr content and distribution, grain size, roughness, environmental conditions, and corrosive media [5, 12–15]. For instance, S. Ghosh et al.

[12] and S. Cissé et al. [16] studied the influence of surface finishing on the corrosion resistance of 304L steel. The corrosion behavior of 304 SS and oxide film properties under different corrosion solutions, temperatures and immersion times has been reported by V. Karki and M. Singh [14], H. Sun et al. [17] and J. Xu et al. [4], respectively.

Until now, previous investigations have been focused on both, the corrosion rate of stainless steels [14, 15, 18–20], and the mechanism of growth, characteristics, and properties of the oxide surface scales formed on SS under a wide variety of corrosive conditions [14, 19, 21–23]. However, the corrosion behavior of as-received, ground, and oxidized 304 SS in NaCl solution saturated with CO_2 has not been reported. Hence, the aim of this study is to evaluate and compare the electrochemical behavior of 304 SS with different superficial and oxidation conditions; and also investigate the ability of the oxide scale formed during pre-oxidation to further mitigate corrosion or instead to determine if the alloy undergoes subsequent degradation.

The results will highlight the differences in the corrosion resistance of as-received, ground, and pre-oxidized 304SS by means of electrochemical techniques including, potentiodynamic polarization, open circuit polarization, linear polarization resistance, and electrochemical impedance spectroscopy combined with structural and microstructural characterizations.

2. EXPERIMENTAL PROCEDURE

2.1. Materials and Characterization Techniques

Commercial AISI 304 SS plates (25.4 × 25.4 × 3 mm) with chemical composition Fe–18.9Cr–8.2Ni–0.9Mn–0.5Si–0.02C (wt %) were employed. The samples were evaluated having two initial surface conditions: as-received and ground, with and without an oxidation treatment. For the ground samples, the grinding process was carried out with a 1000 grit SiC paper. A tubular furnace (GSL-1600X, MTI Corp.) was used to carry out the oxidation treatments at 1100°C for 2 h, in two oxygen partial pressures (pO_2): air (0.21 atm) and argon (1×10^{-5} atm).

The 304 SS samples were characterized by X–ray diffraction (XRD) using a Rigaku Dmax2100 diffractometer with Cu–K_α radiation. The surface of the samples were examined using a scanning electron microscope (SEM, Philips XL30) coupled with an energy-dispersive X-ray spectrometer (EDS) to measure the chemical composition.

7.2. Electrochemical Corrosion Measurements

The corrosion resistance of the 304 SS samples was evaluated in a 3.5 wt % NaCl solution, saturated with CO_2 for 24 h at 50°C. A computer controlled ACM potentiostat was used to carry out the potentiodynamic measurements. The electrochemical studies were performed using a three-electrode cell with a platinum wire and a saturated calomel electrode (SCE) as a counter and reference electrode, respectively. The exposed area of all samples was 1 cm^2. The polarization curves were recorded from –300 to 1000 mV from corrosion potential with a scan rate of 1 mV/s, in accordance to ASTM standards G3-89 and G5-94. The open-circuit potential (OCP) versus a SCE was measured as a function of time. The lineal polarization resistance (LPR) was measured from open circuit region at a constant scanning rate of 1 mV/s from –20 to 20 mV. The electrochemical impedance spectroscopy (EIS) tests were performed under open-circuit conditions using a frequency interval of 100000 to 0.01 Hz and a sinusoidal excitation voltage of ±10 mV.

3. RESULTS AND DISCUSSION

3.1. Stainless Steel Characterization After Oxidation Treatments

X-ray characterization results of the stainless steel in its as-received, ground, and oxidized conditions are presented in Fig. 1. The diffraction pattern of the as-received and ground 304 SS samples presents the peaks corresponding to γ- and α-Fe structures. After 2 h oxidation at 1100°C, Fig. 1a shows that the oxides formed on the surface of the as-received sample oxidized in air are Fe_2O_3 and $(Fe_{0.6}Cr_{0.4})_2O_3$ while on the Ar-oxidized sample, Fe + $2Cr_2O_4$ and traces of $(Fe_{0.6}Cr_{0.4})_2O_3$ appeared. The oxide scale grown on the ground and air-oxidized 304 SS consist of Fe + $2Cr_2O_4$ and traces of Fe_2O_3, and only Cr_2O_3 and $Mn_{1.5}Cr_{1.5}O_4$ phases are identified for the ground sample pre-oxidized in Ar (Fig. 1b).

Although 304 SS has enough chromium to maintain a stable external Cr_2O_3 scale, it has been reported that the formation of the oxide layer onto SS surface depends on several parameters such as temperature, chemical composition, surface condition and oxidation atmosphere [24–27]. During oxidation of stainless steel at high pO_2, chromium and iron oxides can grow at the surface of the stainless steel due to their thermodynamic stability. Chromium is initially oxidized followed by iron [26, 28]. The Fe dissolve in and diffuse through the Cr oxide scale as oxidation time increases; this diffusion is promoted by the high oxygen activity and fast growing rates of Fe-rich oxides at high pO_2 values and also due to the high solubility of Fe and Cr oxides [24, 28]. The Fe incorporates into the Cr scale and transforms into a spinel and eventually, some of the iron ions will diffuse outwards and segregate at the surface forming Fe-rich layers at the outer scale surface [24, 26, 28, 29]. Instead, at low oxygen environments, preferential oxidation of chromium occurs due to its thermodynamic stability [25]. The diffusion and oxidation of Fe is limited or obstructed at these conditions by the low activity of

oxygen in low oxygen partial pressure [26, 28] and by the formation of the most stable and favored oxide (Cr_2O_3) along the entire surface of the alloy [12, 30]. Furthermore, the selective formation of Cr_2O_3 during oxidation is favored on ground surfaces. It has been pointed out that surface treatments such as grinding, machining and cold rolling improve the chromium diffusivity from the metal to the surface of the alloy, thereby increasing the Cr content in the oxide scale formed [12, 31]. The grinding generates a grain size reduction which allows a faster grain boundary diffusion of Cr and therefore chromium oxide formation [12, 30, 32, 33].

The formation of Cr-Mn spinels during oxidation of stainless steel at high temperature has been previously reported [27, 34, 35]. The presence of manganese spinels on the oxide layer is attributed to the high affinity of Mn for oxygen, its faster diffusion rate through Cr_2O_3, and the stability of the spinel at high temperatures [27, 28, 34].

The microstructural characteristics of oxidized 304 SS are shown in Fig. 2. Detailed examination by SEM micrographs shows that different oxide morphology developed under high temperature oxidation. As observed in Fig. 2a, the oxide scale formed on the as-received specimen oxidized in air consists of large polyhedral crystals, which according to the chemical analysis are enriched in iron with small amounts of Cr detected (~8.6 at %). Some porosities are also observed along the surface of the sample. On the contrary, a more compact and regular oxide scale with Cr-rich equiaxial grains and some Fe-rich oxides with blade-like microstructure is observed on the surface of the argon-pre-oxidized sample (Fig. 2b).

After oxidation for 2 h in air, an irregular, porous and cracked oxide microstructure is observed on the ground SS surface (Fig. 2c). The oxide scale formed on this sample shows large areas covered with small and loosely packed polyhedral oxide crystals, rich in Fe (~45 at %), and some flattened zones which according to the chemical analysis are enriched in Cr and Fe (~17 and 18 at %, respectively). On the contrary, after pre-oxidation in argon, a more compact and uniform oxide scale with smooth appearance and with fine and irregularly shaped grains is observed, Fig. 2d. EDS analysis indicated that the dark gray areas are rich in Cr (~32 at %) and the lighter gray grains contained Cr and significant amounts of Mn (~21 and 13.5 at %, respectively). Iron was not detected on the surface of the sample. This oxide is more uniform in composition and shows the highest chromium concentration. This was expected due to at low oxygen partial pressures selective oxidation of Cr is favored while the iron is thermodynamically unstable as pO_2 decreases [25, 26]. Moreover, oxide layers with high Cr content are favored in case of ground or machined conditions as reported by S. Ghosh et al., [12]. It is important to mention that the samples oxidized in air showed spallation during cooling to room temperature whereas no scale spallation was observed on the argon pre-oxidized specimens.

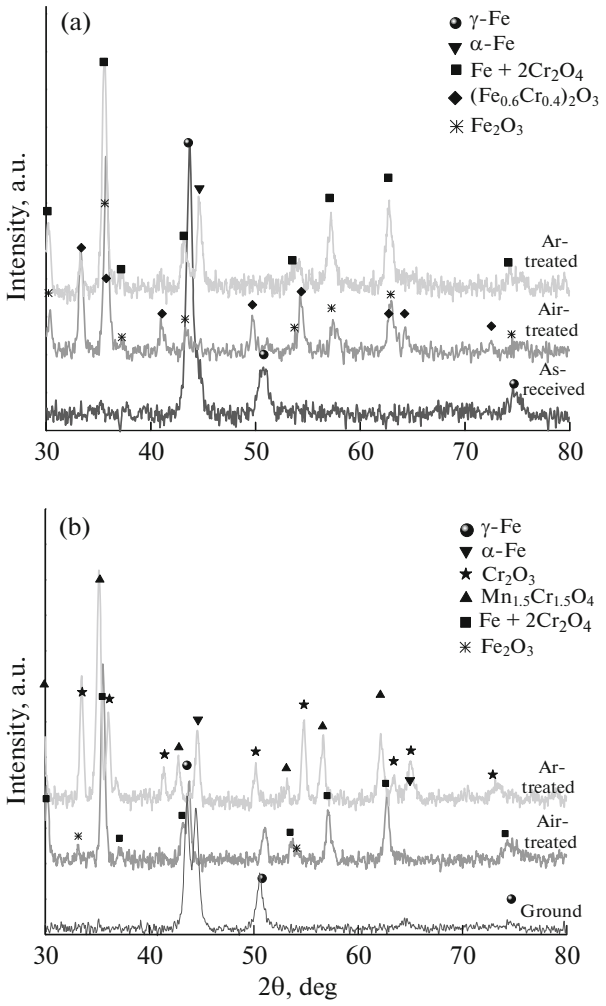

Fig. 1. X-ray diffraction patterns of the stainless steel pre-oxidized in air and argon, (a) without grinding and (b) ground.

3.2. Polarization Curves

Figure 3 presents the active/passive behavior of the samples with different oxidation and surface conditions determined by potentiodynamic polarization curves. The as-received stainless steel has the typical polarization behavior of an active-passive metal with a corrosion potential about −560 mV. In the anodic region a passivation zone is observed between ~−500 to −158 mV. At these potentials, the dissolution rate decreases and remains independent of the potential as a consequence of the growing of a passive layer onto its surface protecting the 304 SS from the corrosion species. As the potential increases the current density increases exponentially. The ground stainless steel shows a low corrosion current density (one order of

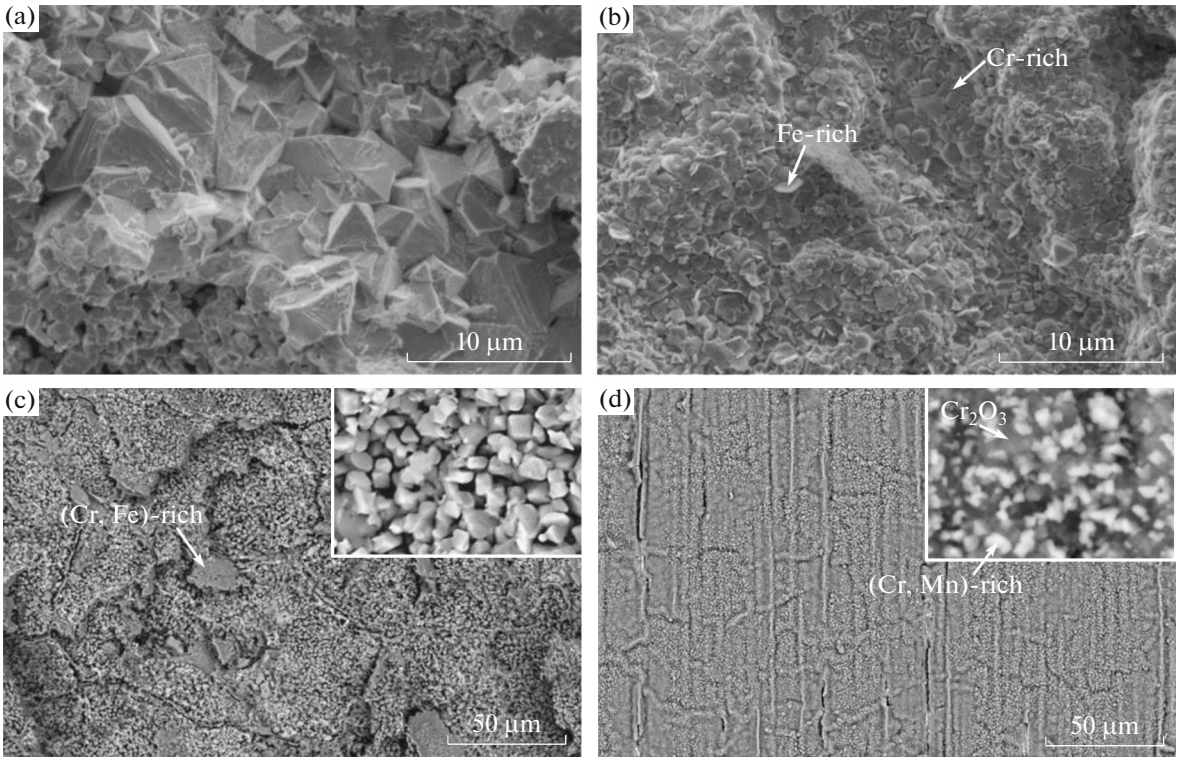

Fig. 2. Surface morphology of 304 SS samples after pre-oxidation treatments; (a) as-received in air, (b) as-received in argon, (c) ground in air, and (d) ground in argon.

magnitude) and a more noble corrosion potential compared to the as-received specimen, however, this sample shows an active-pseudo-passive behavior from −480 to 30 mV, and beyond this point the current density increases exponentially as the potential increases. The nobler corrosion potential and the lower corrosion rate are attributed to the grinding treatment which reduces the active sites and heterogeneities in the surface of the sample and also favors the diffusion of Cr from the SS and therefore the formation of oxide layers with high Cr content [12]. On the contrary, regardless of the surface treatment, a passive region was not observed for the thermally treated 304 SS. The anodic branches of the oxidized samples, except for the ground heat-treated in Ar, are almost the same indicating a similar corrosion behavior. The corrosion potential values of the air-treated samples are similar to the as-received SS while the corrosion potentials of argon oxidized specimens shift slightly toward more active values. This active corrosion process might be related to the oxide scale morphology which increases the surface reaction area due to their roughness and porosity (Fig. 2a, c), the presence of non-protective oxides on the surface of the samples with high dissolution rates in aqueous solutions such as Fe-rich oxides [4], and to the heat treatment which may cause the precipitation of chromium carbides into the alloy. T.M. Devine [36] has found that precipitation of chromium carbide particles caused a Cr-depletion in the outer zone of the alloy changing its chemical composition. This precipitation is harmful to the corrosion resistance of austenitic stainless steels, because they can be susceptible to intergranular corrosion. This corrosion occurs due to a sensitization phenomenon which consists of Cr-depletion zones adjacent to Cr-rich precipitates, such as $M_{23}C_6$ carbides [36].

Table 1 summarizes the electrochemical parameters results for the 304SS samples with different condition applying the Tafel extrapolation method. According to the results, the ground specimen presents the best performance in aqueous solution at the beginning of the corrosion process whereas the Tafel extrapolation suggests a faster corrosion rate for the oxidized samples. Analyzing the values of the cathodic Tafel slope (B_c), it is observed that as the pO_2 decreases the B_c values increases. This might imply that the mass transfer processes of electrolyte to the reaction surface are affected by the oxidation conditions.

3.3. OCP vs Time Measurements

The corrosion potential curves as a function of time for all 304 SS samples evaluated in a CO_2-saturated 3.5% NaCl solution are presented in Fig. 4. A similar behavior is observed for the as-received and ground specimens. The increase of the potential within the first hours of the test is associated to the formation of

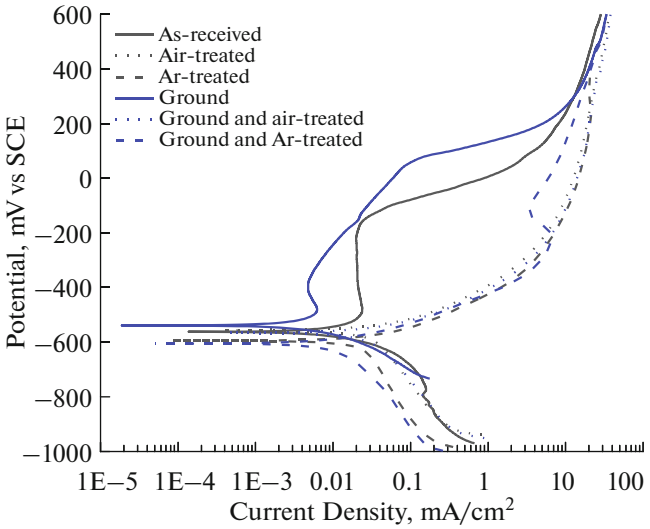

Fig. 3. Potentiodynamic polarization curves of the 304 stainless steel samples with different oxidation and surface treatment.

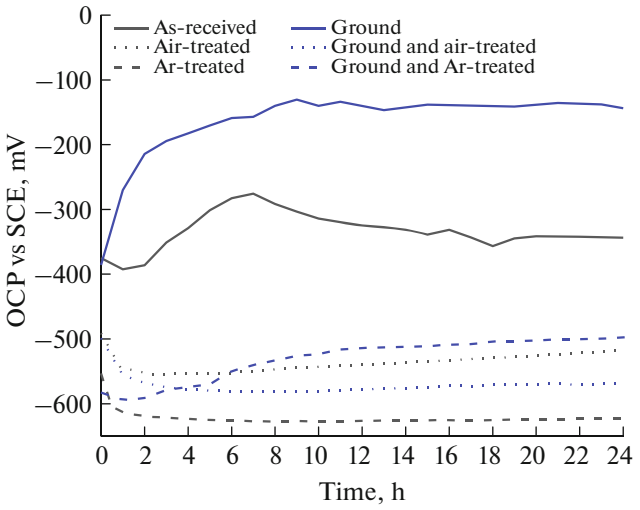

Fig. 4. Change of OCP as a function of time of the samples exposed to NaCl solution saturated with CO_2.

a passive layer on the surface of the samples, and the steady potential reached afterward indicates that these layers remain protective and stable [37]. However, the ground stainless steel sample shows a significant increase and the noblest OCP throughout the corrosion test which indicates high corrosion resistance. This is attributed to the grinding process which generates a homogeneous surface and also favors the growth of a stable protective oxide [12]. Analogous to the polarization results, more active corrosion potentials are obtained for the samples subjected to oxidation regardless its surface condition. Contrary to the OCP of the as-received and ground samples, the potential decreases within the first hours (0 to 3) and afterward approaches stabilization except for the air-treated and the ground + Ar-treated samples where the OCP shifts slightly to more noble values to the end of the test. Even though the oxidized SS presented the more active potentials, the stability reached after 3–4 h evidences that the oxide layer formed during the oxidation treatments seems to remain protective towards the end of the test.

The most active behavior of the oxidized samples compared to the non-oxidized specimens is attributed to the greater surface area as a result of the thermally grown oxide onto the samples surface, dissolution or poor stability of non-protective oxides, the porous morphology of the oxide layer which allows the penetration of the aqueous solution (e.g. Fig. 2c), and Cr-depletion. As mentioned before, the heat treatment caused oxidation of Cr generating a Cr-depletion region in the outer zone of the alloy. This depletion is detrimental to the 304 SS because the corrosion resistance of these alloys are highly depend on the chromium content [5, 24, 38].

The more noble corrosion potential values of the ground sample pre-oxidized in Ar, respect to the samples exposed to oxidation, is related to its high Cr percentage contained in the surface (~30 at %) and a more compact thermally grown oxide. It has been well established that low pO_2 decreases the oxidation rates and then inhibits the formation of oxides with high growth rates (Fe-rich oxides) and favors those with low oxidation rates such as Cr_2O_3 [26, 28].

Table 1. Electrochemical parameters of the samples evaluated in CO_2-saturated brine at 50°C

Sample	E_{corr}, mV	I_{corr}, mA/cm^2	B_a, mV/Dec	B_c, mV/Dec
As-received	−560	0.0140	192	123
Air-treated	−555	0.0310	150	388
Ar-treated	−595	0.0237	122	465
Ground	−539	0.0027	116	178
Ground and air-treated	−565	0.0318	90	352
Ground and Ar-treated	−603	0.0173	98	394

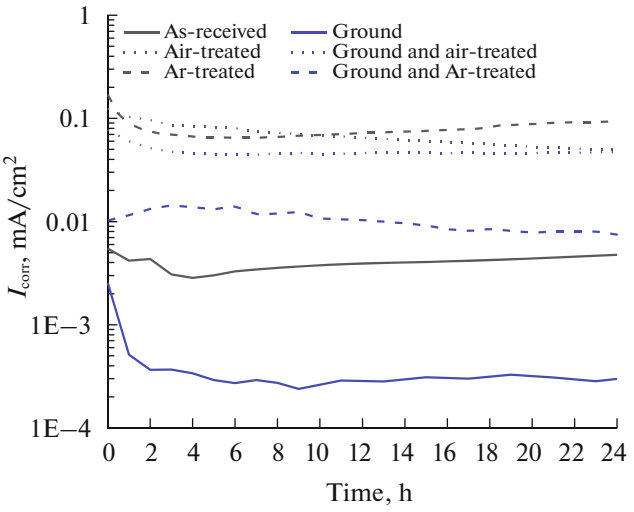

Fig. 5. I_{corr} versus immersion time of the 304 SS exposed to CO_2-saturated solution.

3.4. LPR Measurements

The results of I_{corr} measurements versus time are plotted in Fig. 5. All samples show a decrease in the I_{corr} values within the first hours in contact with the electrolyte, except the ground specimen heat-treated in Ar. After this period, the ground and ground + air-treated samples reached a steady state, the corrosion current of both air-treated and ground sample oxidized in argon slightly decreases with time while a gradual increase of the I_{corr} is observed for the as-received and the Ar-oxidized SS. This increase suggests penetration of the corrosion solution while the decrease indicates a passive behavior [4, 39].

As observed in Fig. 5, the ground 304 SS sample showed the lowest corrosion rates of all conditions evaluated. Oxidation treatments decreased the corrosion resistance of stainless steel; an increase of almost three orders of magnitude in the I_{corr} values is observed. As already indicated, during the oxidation treatments, a solely oxide scale (Cr_2O_3) onto the alloy surface was not formed, and the growing of oxides with porous and cracked morphology increase the surface reaction area. Moreover, the formation of iron rich oxides instead of Cr_2O_3 increases the corrosion rate of the 304 SS due to the preferential dissolution of iron [4, 21, 40]. Similar to the OCP results, the intermediate behavior of the ground + Ar treated is attributed to the formation of an oxide scale with a more uniform morphology and lower superficial defects (pores and microcracks) composed predominantly by chromium. These results agreed with the polarization curves and OCP values where the samples without oxidation treatment showed lower corrosion rates than those subjected to an oxidation treatment.

3.5. Electrochemical Impedance Spectroscopy Measurements

Bode diagrams for the as-received and heat-treated in air and argon 304 SS are shown in Fig. 6. From Fig. 6a, c, e, it is observed that at high frequency, $f > 1000$ Hz, the samples exhibit a plateau of $|Z|$ as the phase angle approaches to zero. This is the response of the solution resistance, R_s, and includes the cell geometry, electrolyte resistance, impedance of the conductors and the reference electrode.

Generally, in the middle frequency region (1000 to 10 Hz), an ideal diagram shows a linear slope of about -1 in $\log|Z|$ as $\log(f)$ decreases and a maximum phase angle (~$-90°$). This behavior is related with the capacitive response of the electrode and defines the dielectric properties of the electronically conducting surface layer. A phase angle greater or equal to 90° indicates that the protective layer is an effective insulating film; hence there is no current leakage at defect sites. On the contrary, if the phase angle is less than 90° then the protective layer is permeable to ions from solution [41]. In the present cases, the maximum phase angle was observed at frequencies below 10 Hz, where the as-received 304 SS showed the maximum value around 70°, and remained practically stable throughout the test (Fig. 6b). The phase angle increased from 47 to 53° for the sample oxidized in air, and in the case of the 304 SS oxidized in argon, the phase angle remained constant around 47°, but with a shift at lower frequencies, Fig. 6d, f, respectively. This behavior can be related to the presence of a thin protective layer onto the stainless steel surface, where for the as-received 304 SS, this layer showed the best dielectric properties. In the case of the sample oxidized in air, the protective film tends to improve their protective capacity while the displacement of the phase angle spectrum toward lower frequencies of the 304 SS oxidized in argon may be associated with detachment or thinning of the protective scale [42].

Similar to the high frequency region, in the low frequency region ($f < 10$ Hz), the Bode plot exhibits a plateau of $|Z|$ as the phase angle approaches to 0°. The electron charge and mass transfer processes, as well as other relaxation processes arising at the film-electrolyte interface or within the pores of the surface layer are identified in this region [43]. However, from Fig. 6, both the plateau and the phase angle approaching to 0° occur at lower frequencies than 0.01 Hz. The analysis shows that in all cases only one time constant is observed, which corresponds to the characteristic response of a protective film developed onto the stainless steel surface. The maximum $|Z|$ value is obtained by the as-received 304 SS, followed by the pre-oxidized in air 304 SS, and the lowest $|Z|$ value was observed for oxidized steel in argon.

Respect to 304 SS samples with grinding process, it is observed from Fig. 7 that both, the ground 304 SS and the ground + air-oxidized sample showed very

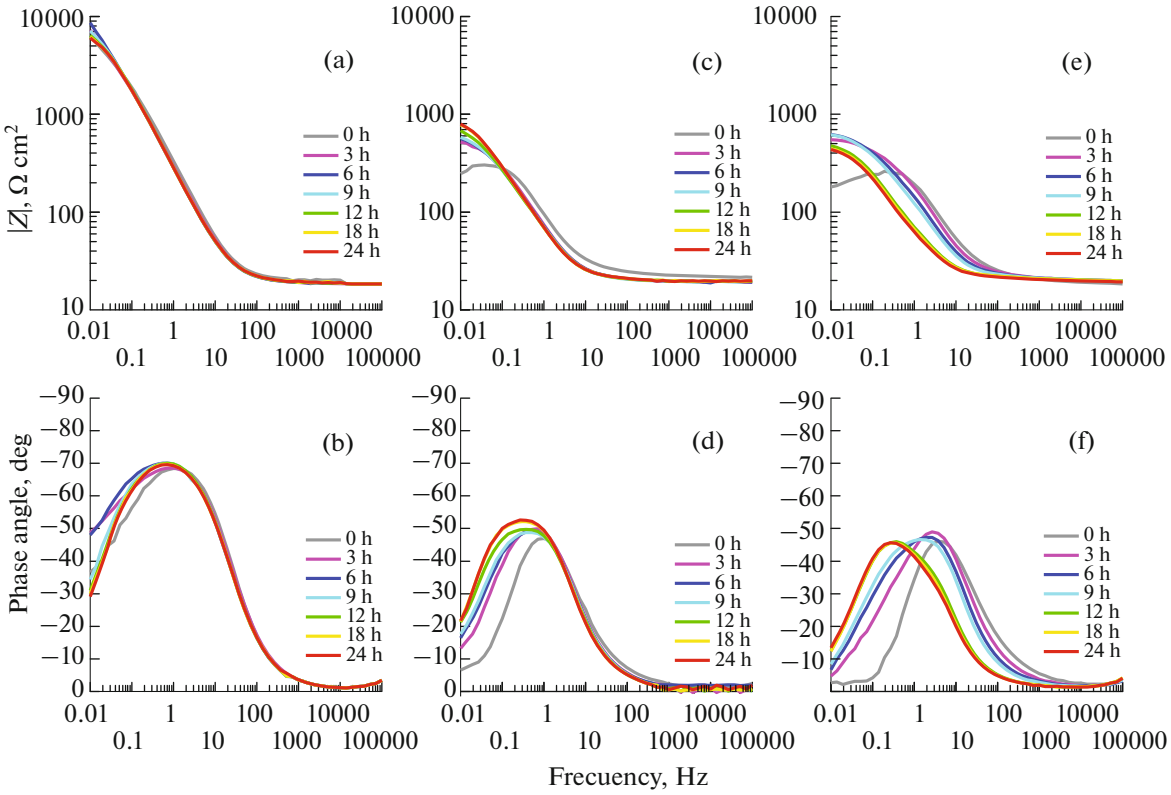

Fig. 6. Bode plots for as-received 304 SS with different condition; (a, b) without pre-oxidation, (c, d) pre-oxidized in air, and (e, f) pre-oxidized in argon.

similar impedance spectra (Figs. 7a–7d) to those observed for the same steels but without grinding (Figs. 6a–6d). However, the ground 304 SS showed the maximum phase angle value (77°) in correspondence with an increase in the impedance module at lower frequencies. Regarding the ground sample pre-oxidized in argon, this specimen showed a different behavior; according to the evolution of the phase angle the presence of two time constants are observed, Fig. 7f. One of them between the high-intermediate frequency region and the second one in the low frequency region. It is remarkable that the magnitude and position of the second one is very similar to that observed for the same material but without grinding (Fig. 6f). This may indicate that the presence of the first time constant is responsible for the increase observed in the corrosion resistance, according to the magnitude of $|Z|$ (two orders of magnitude).

In general, in the CO_2-corrosion process, CO_2 dissolves in water to form carbonic acid, and this result in acidic brine that causes general corrosion or a localized attack on the metal surface. In the case of carbon steel corrosion, an iron oxide layer is formed which is an active form of corrosion since corrosion continues after the film has formed, but the formation and precipitation of $FeCO_3$ onto metal surface increase its corrosion resistance. It has also been suggested that additions of chromium decrease the corrosion rate of Cr-modified steels, respect to carbon steel, as a result of the presence of more stable passive films with better protective properties and repassivation rate and to the microstructural changes of the film of the corrosion product [9, 44]. However, in the corrosion process of stainless steel a passive corrosion layer is formed, which stops corrosion. This layer self-healed quickly when damaged but it can deteriorate depending on the temperature, chlorides and, pH. In general, Fe and Cr oxides are the main components in the oxide film formed on stainless steel, but according to the enrichment factor, Cr is enriched in the oxide film while Fe is depleted. Because Cr_2O_3 is not complexed by dissolved CO_2, the Cr-enrichment of the passive film is achieved by the dissolution of the Fe oxide, i.e., in the passive state, the rate is controlled by dissolution of Fe through the already passive surface and by very slow dissolution of the passivating chromium oxide itself [45].

It has been reported that in acidic brines, one of the primary constituents of the outermost layer of the protective films formed onto stainless steel is $Cr(OH)_3$ [46]. Then, the anodic corrosion process of the stainless steel primarily implies dissolution and growth of passive film according the following [39, 47]:

$$Cr + 3H_2O \rightarrow Cr(OH)_3 + 3H^+ + 3e^-,$$

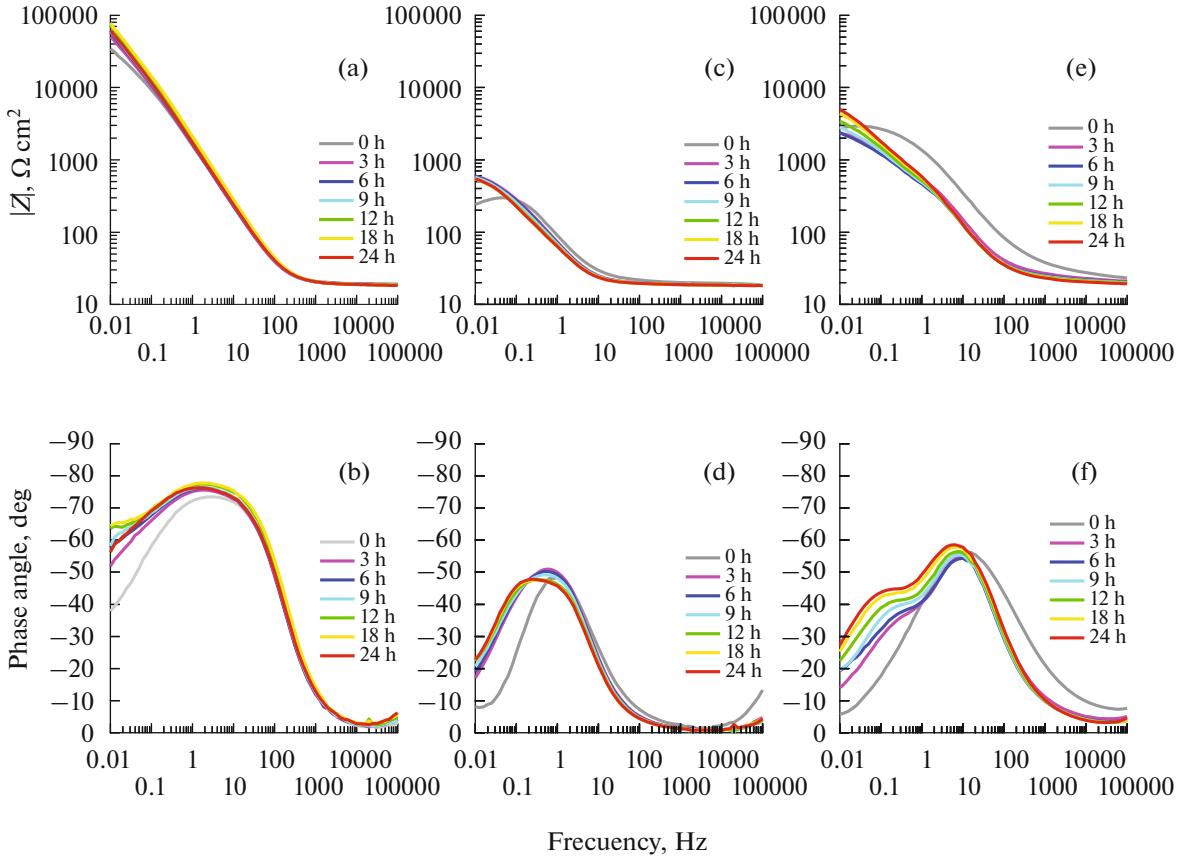

Fig. 7. Bode plots for ground 304 stainless steel with different condition (a, b) non-oxidized, (c, d) air-oxidized, and (e, f) Ar-oxidized.

$$Cr^{3+} + 3H_2O \leftrightarrow Cr(OH)_3 + 3H^+.$$

Other possible corrosion process is given by the following reaction [47]:

$$Fe^{2+} + CO_3^{2-} \rightarrow FeCO_3,$$

$$Fe + HCO_3^- \rightarrow FeCO_3 + H^+ + 2e^-.$$

According to the previous explanation, it can be established that the behavior observed in the case of as-received and ground 304 SS (both without pre-oxidation), is due to the rapid establishment of a Cr-rich protective oxide which increased the capacitive properties of the surface. In case of the as-received 304 SS pre-oxidized in both air and argon, as well as the ground 304 SS pre-oxidized in air, the observed behavior can be associated with a dissolution process of the oxides and spinels present onto the surface of the samples. On the other hand, the ground 304 SS pre-oxidized in argon (two time constants) its behavior is due to the presence of a protective layer based mainly in Cr, where the time constant observed at the high-intermediate frequency region corresponds to formation and precipitation of $Cr(OH)_3$ on the surface. As a result, its corrosion resistance was higher (two orders of magnitude) respect to the other pre-oxidized samples.

Figure 8 compares the microstructure of ground 304 SS pre-oxidized in air and argon exposed to CO_2-saturated solution during 24 h. As observed in Fig. 8a, the oxide of the stainless steel pre-oxidized in air appears similar to the non-corroded specimen, however, a detail examination of the surface shows that the polyhedral crystals are not visible and instead relatively flat zones and areas covered with remnants of crystals are observed. In contrast, a more homogeneous oxide layer with fine grains still covers the surface of the sample heat-treated in Ar (Fig. 8b). High Cr content (~30 at %) and significant quantities of Mn (10 at %) are still detected by EDS on the surface of this sample. The chemical composition results of the pre-oxidized in air indicate that the Cr content increased (from 17 to 25 at %) but a significant decrease in Fe content, from 45 to 14 at %, is detected respect to the uncorroded specimen. This confirms the results observed in the electrochemical measurements. In terms of corrosion resistance under CO_2-saturated brine solutions, Cr-rich protective layers showed a higher corrosion resistance whereas a preferential dissolution process occurred in those protective

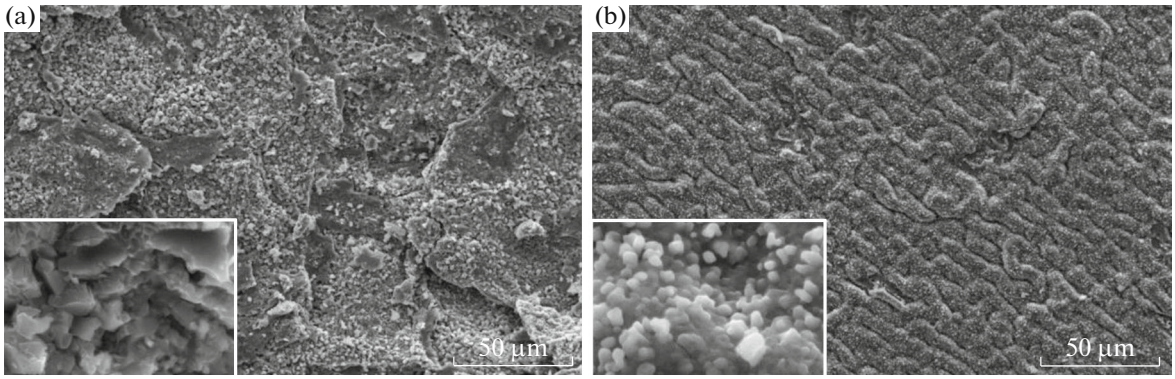

Fig. 8. Surface morphology of ground samples heat-treated in (a) air and (b) argon atmospheres after exposure to CO_2-saturated solution.

layers formed by multiple oxides increasing the corrosion rate.

4. CONCLUSIONS

The oxidation behavior of the stainless steel is attributed to a synergistic effect of the pre-oxidation atmosphere and surface condition.

The formation of a protective layer of Cr_2O_3 is promoted on the surface of the ground SS during oxidation in argon. Heat-treatments in air resulted in the formation of fast-growing Fe-rich oxides.

The grinding process have a positive effect on the low temperature corrosion performance of 304 stainless steel because decreases surface defects and active sites and also favors the growing and formation of Cr_2O_3 under low pO_2.

Oxidation treatments increase the corrosion susceptibility of stainless steel in chloride environment. However, this acceleration is strongly related with the microstructural characteristics of the oxide scale formed. Cr-oxides with dense characteristics respond competitively in terms of corrosion resistance under CO_2-solutions. Oxide scales with a porous a non-homogeneous morphology allow penetration of ions from the solution.

The diminution of Fe content on the surface of the corroded samples evidence its susceptibility to dissolution when exposed to NaCl solution saturated with CO_2.

Nevertheless the oxidized stainless steel present higher corrosion rates, the oxidation conditions which are capable to protect 304 stainless steel are those that generate the formation of a slow-growing and stable Cr-oxide with few microstructural defects.

FUNDING

Financial support from CONACYT-Mexico is gratefully acknowledged. The authors also thank to the Catedras program and to the National Laboratories CENAPROT and LIDTRA, for providing all the facilities required to carrying out this work.

The authors declare no conflict of interest.

REFERENCES

1. Lo, K.H., Shek, C.H., and Lai, J.K.L., *Mater. Sci. Eng.,* 2009, vol. 65, p. 39.
2. Lima, A.S., Nascimento, A.M., Abreu, H.F.G., and De Lima-Neto, P., *J. Mater. Sci.,* 2005, vol. 40, p.139.
3. Sahin, S. and Übeyli, M., *J. Fusion Energy,* 2008, vol. 27, p. 271.
4. Xu, J., Wu, X., and Han, E.H., *Electrochim. Acta,* 2012, vol. 71, p. 219.
5. Terachi, T., Yamada, T., Miyamoto, T., and Arioka, K., *J. Nucl. Sci. Technol.,* 2008, vol. 45, p. 975.
6. Townsend, H.E., *Corrosion*, 2001, vol. 57, p. 497.
7. Bojinov, M., Kinnunen, P., Lundgren, K., and Wikmark, G., *J. Electrochem. Soc.,* 2005, vol. 152, p. B250.
8. Perez, T.E., *JOM,* 2013, vol. 65, p. 1033.
9. Banaś, J., Lelek-Borkowska, U., Mazurkiewicz, B., and Solarski, W., *Electrochim. Acta,* 2007, vol. 52, p. 5704.
10. Kermani, M.B. and Morshed, A., *Corrosion,* 2003, vol. 59, p. 659.
11. Ziemniak, S.E., Hanson, M., and Sander, P.C., *Corros. Sci.,* 2008, vol. 50, p. 2465.
12. Ghosh, S., Kumar, M.K., and Kain, V., *Appl. Surf. Sci.,* 2013, vol. 264, p. 312.
13. Rees, E.E., McPhail, D.S., Ryan, M.P., Kelly, J., and Dowsett, M.G., *Appl. Surf. Sci.,* 2003, vols. 203–204, p. 660.
14. Karki, V. and Singh, M., *Int. J. Mass Spectrom.,* 2017, vol. 421, p. 51.
15. Zheng, Z.B. and Zheng, Y.G., *Corros. Sci.,* 2016, vol. 112, p. 657.
16. Cissé, S., Laffont, L., Tanguy, B., Lafont, M.C., and Andrieu, E., *Corros. Sci.,* 2012, vol. 56, p. 209.
17. Sun, H., Wu, X., and Han, E.H., *Corros. Sci.,* 2009, vol. 51, p. 2840.

18. Tsutsumi, Y., Nishikata, A., and Tsuru, T., *Corros. Sci.,* 2007, vol. 49, p. 1394.
19. Sim, J.H., Kim, Y.S., and Cho, I.J., *Nucl. Eng. Technol.,* 2017, vol. 49, p. 769.
20. Cuevas Arteaga, C., Porcayo Calderón, J., Campos Sedano, C.F., and Rodríguez, J.A., *Int. J. Electrochem. Sci.,* 2012, vol. 7, p. 445.
21. Kuang, W., Wu, X., and Han, E., *Corros. Sci.,* 2010, vol. 52, p. 4081.
22. Carmezim, M.J. and Simo, A.M., *Corros. Sci.,* 2005, vol. 47, p. 581.
23. Sun, M., Wu, X., Zhang, Z., and Han, E., *Corros. Sci.,* 2009, vol. 51, p. 1069.
24. Birks, N., Meier, G.H., and Pettit, F., *Introduction to the High-Temperature Oxidation of Metals*, New York: Cambridge Univ. Press, 2006.
25. Baer, D.R., *Appl. Surf. Sci.,* 1981, vol. 7, p. 69.
26. Huntz, A.M., Reckmann, A., Haut, C., and Herbst, M., *Mater. Sci. Eng., A,* 2007, vol. 447, p. 266.
27. Wild, R.K., *Corros. Sci.,* 1977, vol. 17, p. 87.
28. Young, D.J., *High Temperature Oxidation and Corrosion of Metals,* London: Elsevier, 2008.
29. Whittle, D.P. and Wood, G.C., *J. Electrochem. Soc.,* 1967, vol. 114, p. 986.
30. Yurek, G.J., Eisen, D., and Garratt-Reed, A., *Metall. Trans. A,* 1982, vol. 13, p. 473.
31. Kain, V., Chandra, K., Adhe, K.N., and De, P.K., *J. Nucl. Mater.,* 2004, vol. 334, p. 115.
32. Merz, M.D., *Metall. Trans.,* 1979, vol. 10, p. 71.
33. Peng, X., Yan, J., Zhou, Y., and Wang, F., *Acta Mater.,* 2005, vol. 53, p. 5079.
34. Stott, F.H., Wei, F.I., and Enahoro, C.A., *Werkst. Korros.,* 1989, vol. 40, p. 198.
35. Riffard, F., Buscail, H., Caudron, E., Cueff, R., Issartel, C., and Perrier S., *Mater Charact.,* 2002, vol. 49, p. 55.
36. Devine, T.M., *Corros. Sci.,* 1990, vol. 30, p. 135.
37. Gurappa, I., *Mater. Charact.,* 2002, vol. 49, p.73.
38. Chen, C.F., Lu, M.X., Sun, D.B., Zhang, Z.H., and Chang, W., *Corrosion,* 2005, vol. 61, p. 594.
39. Kargar, B.S., Moayed, M.H., Babakhani, A., and Davoodi, A., *Corros. Sci.,* 2011, vol. 53, p. 135.
40. Kocijan, A., Crtomir, D., and Jenko, M., *Corros. Sci.,* 2007, vol. 49, p. 2083.
41. Lakshminarayanan, V. and Sur, U.K., *J. Phys.,* 2003, vol. 61, p. 361.
42. Porcayo-Calderon, J., Casales-Diaz, M., Rivera-Grau, L.M., Ortega-Toledo, D.M., et al., *J. Chem.,* 2014, vol. 2014, p. 1.
43. Beverskog, B., Bojinov, M., Englund, A., Kinnunen, P., et al., *Corros. Sci.,* 2002, vol. 44, p. 1901.
44. Cheng, Y.F., Bullerwell, J., and Steward, F.R., *Electrochim. Acta,* 2003, vol. 48, p. 1521.
45. Linter, B.R. and Burstein, G.T., *Corros. Sci.,* 1999, vol. 41, p. 117.
46. Liu, C.T. and Wu, J.K., *Corros. Sci.,* 2007, vol. 49, p. 2198.
47. Zhang, H., Zhao, Y.L., and Jiang, Z.D., *Mater. Lett.,* 2005, vol. 59, p. 3370.